Corrosion behavior of pure metals (Ni and Ti) and alloys (316H SS and GH3535) in liquid GaInSn

Jianhui Yu[1, 2], Hongxia Xu[2], Xiangxi Ye[2], Bin Leng[2], Hanxun Qiu[1], Xingtai Zhou[2]

1 School of Materials and Chemistry, University of Shanghai for Science and Technology, Shanghai 200093, China
2 Shanghai Institute of Applied Physics, Chinese Academy of Sciences, Shanghai 201800, China

* Corresponding author: E-mail: xuhongxia@sinap.ac.cn, zhouxingtai@sinap.ac.cn, hxqiu@usst.edu.cn,

Abstract: In this study, the interactions between a Ga-based liquid metal,GaInSn, and several metal materials, including pure metals (Ni and Ti) and alloys (316H stainless steel (SS) and GH3535), at 650 °C were investigated. The aim was to evaluate the corrosion performance and select a suitable candidate material for use as a molten salt manometer diaphragm in thermal energy storage systems. The results indicated that the alloys (316H SS and GH3535) exhibited less corrosion than pure metals (Ni and Ti) in liquid GaInSn. Ga-rich binary intermetallic compounds were found to form on the surfaces of all the tested metal materials exposed to liquid GaInSn, as a result of the decomposition of liquid GaInSn and its reaction with the constituent elements of the metal materials. The corrosion mechanism for all the tested materials exposed to liquid GaInSn was also investigated and proposed, which may aid in selecting the optimal candidate material when liquid GaInSn is used as the pressure-sensing medium.

Keywords: Metal materials, Liquid GaInSn, Corrosion, Intermetallic compounds, Thermal energy storage systems

1 Introduction

In recent years, Ga-based liquid metals (GLMs) have received widespread

attention owing to the emergence of soft robots [1], magnetically active solid–liquid transformation machines [2], and the potential applications of wearable and flexible electronic devices in the medical field [3]. This novel type of multifunctional material possesses metal conductivity and liquid fluidity at room temperature, making it a popular subject of study [4–9].

GaInSn, a GLM material, is considered a key candidate material for sensors in wearable and stretchable electronic devices because of its advantages, such as low toxicity, low melting point, high conductivity/thermal properties, ultralow vapor pressure, and fluidity [10-12]. Several research groups have investigated the development and application of GaInSn-based devices. Matsuzaki et al. [3] fabricated a GaInSn sensor electrode for wearable devices that could simultaneously sense dispersed local and global strains. Li et al. [13, 14] and Zhang et al. [15] produced Ga_2O_3-, GaN-, In_2O-, and SnO-based devices as well as other electronic devices using room-temperature-based liquid metal printing of electronics and semiconductors, which has injected new vitality into the semiconductor manufacturing industry. He et al. [16] reported an elastic composite consisting of light liquid metal foam spheres (LMSs) with lenticular contact and polydimethylsiloxane and systematically studied the interface contact conduction mechanism and strain sensitivity between LMSs with different melting points. Their results showed that the composite has potential applications in biomedicine and industry. So et al. [17] reported a method for manufacturing reversible and adjustable fluid antennas from a GLM with a radiation efficiency reaching 90% in

far-field measurements. Shirzadi et al. [18] reported that Ga could be used to remove the native oxide layer during the grinding of the jointing faces of 304 SS and Ti prior to diffusion bonding experiments.

Recently, GaInSn was selected as the pressure-conducting medium in the molten salt manometer of thermal energy storage (TES) systems. However, the material for the pressure-sensing diaphragm has not yet been chosen. One crucial issue that must be addressed for pressure-sensing diaphragms is the possibility of corrosion hardening or embrittlement caused by long-term contact between liquid GaInSn and metallic elements, such as Ni, Fe, Cr, and Mo, resulting in pressure conduction failure. The mechanisms of corrosion and failure may be related to the elemental dissolution of the pressure-sensing diaphragm when directly exposed to a GLM environment or the simultaneous formation of Ga-rich intermetallic compounds (IMCs). Therefore, the most crucial characteristic of the pressure-sensing diaphragm material is its excellent corrosion resistance to the GLM, which ensures the safe operation of the molten salt pressure gauge.

316H SS is a widely used Fe-based structural material in fields such as the petroleum, chemical, electric power, aerospace, transportation, and energy industries owing to its favorable comprehensive performance, including high-temperature resistance, corrosion resistance, oxidation resistance, high strength, ease of processing, and cost-effectiveness. 316H SS is a leading structural material candidate for TES systems [19, 20]. According to the literature [21–23], the corrosion of 316H SS in chloride salts, the heat storage medium used in TES

systems, primarily manifests as the oxidation or dissolution of Fe. The GH3535 alloy, which is the Chinese version of the UNS N10003 alloy [24], is a solid-solution-strengthened nickel-based alloy selected as the main candidate structural material for molten salt reactors (MSRs). MSRs are one of the six most promising Generation IV nuclear reactors worldwide [25]. Previous studies have shown that the UNS N10003 alloy has superior corrosion resistance in molten fluorine salts [26–29], and that corrosion is generally caused by the dissolution of Cr from the alloy into fluorine salts. However, the corrosion resistance and stability of materials are affected by various factors, including impurities in the corrosive solvent [26–28] and factors such as coatings [29], elemental additives [30], and segregation of impurities on the grain boundaries (GBs) [31].

However, because liquid metal corrosion (LMC) involves many factors such as element dissolution, diffusion, and chemical reactions, it is more complex than molten salt corrosion. Consequently, very few systematic studies have investigated the corrosion behavior of various metallic materials in liquid metals. Barbier et al. [32] and Shin et al. [33] reported that 316L austenitic stainless steel was severely corroded in a GLM. However, they did not compare the corrosion properties of various materials in the GLM or propose a candidate material with better corrosion resistance. Guo et al. [34] studied the corrosion behavior of T91 steel in liquid GaInSn and found that an $FeGa_3$ reaction film formed at 400 °C could provide better boundary lubrication performance. As reported previously, Ti exhibits minimal corrosion when exposed to Ga in the air at 220 °C [35]. Moreover, pure Ni

is widely acknowledged as an optimal corrosion-resistant coating material in molten salt environments [26, 29]. Nevertheless, it is important to note that pure Ni is susceptible to severe corrosion in GLMs [32]. Thus, we investigated the corrosion behaviors of pure Ti and Ni, providing a valuable reference for our study. It is necessary to evaluate the corrosion behavior of metals or alloys in liquid GaInSn and select a suitable pressure-sensing diaphragm before using it in the molten salt manometers of TES systems.

In this study, the interactions between liquid GaInSn and various materials, including pure metals (Ni and Ti) and alloys (316H SS and GH3535 alloy) were investigated by conducting a static immersion test at 650 °C for 5 h. After LMC, changes in the mass, phase structure, and morphology of the metals and alloys were characterized using weighing, X-ray diffraction (XRD), scanning electron microscopy (SEM), and energy dispersive spectroscopy (EDS) techniques. Based on the corrosion behavior of the tested materials in GaInSn, the corresponding corrosion mechanism was then investigated and proposed.

2 Experimental

2.1 Materials

Table 1 lists the chemical compositions of the pure metals (Ni and Ti) and alloys (316H SS and GH3535) used in this study. These data were provided by the metal suppliers. The surfaces of all the samples were mechanically ground with silicon carbide (SiC) paper to 2000 grit. After polishing, all samples were ultrasonically cleaned with ethanol and dried before the corrosion test. The

composition of GaInSn used in the corrosion experiments is shown in Table 2.

Table 1 Chemical compositions of pure metals (Ni and Ti) and alloys (316H SS and GH3535) (wt.%).

	Fe	Ni	Mn	Ti	Si	P	Cr	Mo	C
Ni	0.07	99.58	0.23	0.07	0.05	-	-	-	-
Ti	0.01	-	0.14	99.85	-	-	-	-	-
316H	base	10.04	1.08	-	0.47	0.04	16.24	2.07	0.06
GH3535	4.03	base	0.77	<0.01	0.59	-	7.03	17.10	0.02

Table 2 Chemical composition of GaInSn (wt.%).

Element	Ga	In	Sn
Wt.%	68.5	21.5	10

2.2 Static corrosion test

A schematic of the corrosion test setup is shown in Fig. 1. First, specimens of Ni (8.0 mm × 8.0 mm × 2.0 mm), Ti (10.0 mm × 8.0 mm × 1.2 mm), 316 H SS (10.0 mm × 8.0 mm × 2.0 mm), and GH3535 alloys (9.0 mm × 9.0 mm × 2.0 mm) were placed into quartz tubes with dimensions of 250 mm (length) × 20 mm (diameter). An equal amount of liquid GaInSn was then dropped into each quartz tube using a syringe to ensure that the liquid GaInSn completely covered the metallic materials. Before vacuum sealing, the quartz tubes were preheated with a flame spray gun for several seconds to remove moisture inside. They were then evacuated to a vacuum pressure of approximately 10^{-4} Pa and sealed with a flame spray gun.

After the vacuum-sealing process was completed, sealed quartz tubes containing various metallic specimens and GaInSn were placed vertically inside a furnace to ensure that the specimens were completely submerged in liquid GaInSn during the test. The specimens were then heated at 650 °C for 5 h. After heating, the quartz tubes were cooled to 23 °C and broken to remove the specimens. The corroded samples were then ultrasonically cleaned with ethanol to remove residual GaInSn from their surfaces.

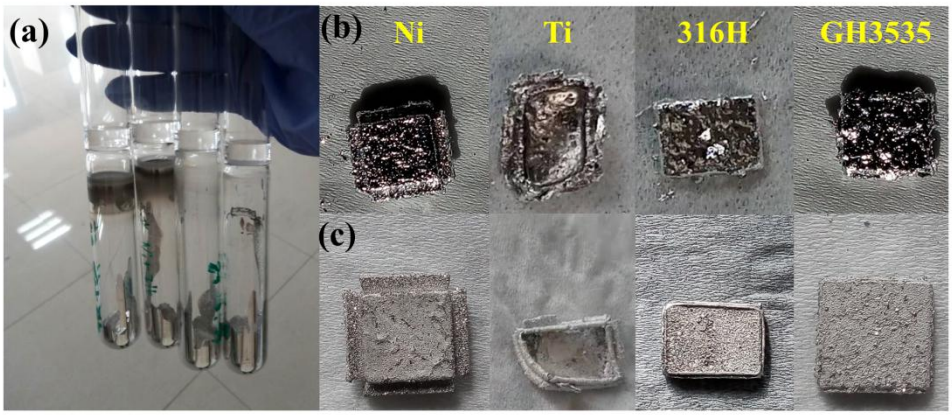

Fig. 1. (a) Schematic diagram of LMC. (b) Samples after corrosion but before cleaning, and (c) samples after cleaning.

2.3 Characterization method

The mass of all samples was measured using an analytical balance (METTLER TOLEDO MS105DU) with an accuracy of 0.01 mg before and after the corrosion test. The weight gain ratio γ for each sample was calculated with the following equation: $\gamma = (W_1-W_0)/W_0$, where W_0 and W_1 represent the mass of each sample before and after corrosion, respectively.

The crystal structure of the samples before and after the corrosion experiment was characterized using an XRD spectrometer (Bruker D8) with a Cu Kα1 radiation source (λ = 0.154 nm).

The surface morphologies and elemental distributions of the samples before and after the corrosion experiments were analyzed using SEM (LEO 1530 V P) and EDS.

3 Results

Figs. 1(b) and (c) show the specimens exposed to GaInSn, revealing the strong adhesion of GaInSn to the surface of the metallic materials after the corrosion test. After cleaning, the corrosion phenomenon and degree of corrosion of the materials exposed to GaInSn at 650 °C for 5 h were found to be distinct from each other and were analyzed separately as described below.

To compare the degree of corrosion of the four types of materials directly, the weight gain ratio γ of each material exposed to GaInSn after the corrosion test was calculated, as shown in Fig. 2. The weight of all the specimens immersed in GaInSn increased after corrosion, indicating a reaction between GaInSn and the metallic materials during immersion. Furthermore, the average weight gain ratio of

the pure metals (Ni: 62.17% and Ti: 150.00%) was significantly larger than that of the alloys (316H SS: 13.71% and GH3535: 12.68%), reflecting the considerably more severe corrosion of the pure metals (Ni and Ti) compared to the alloys (316H SS and GH3535) in liquid GaInSn.

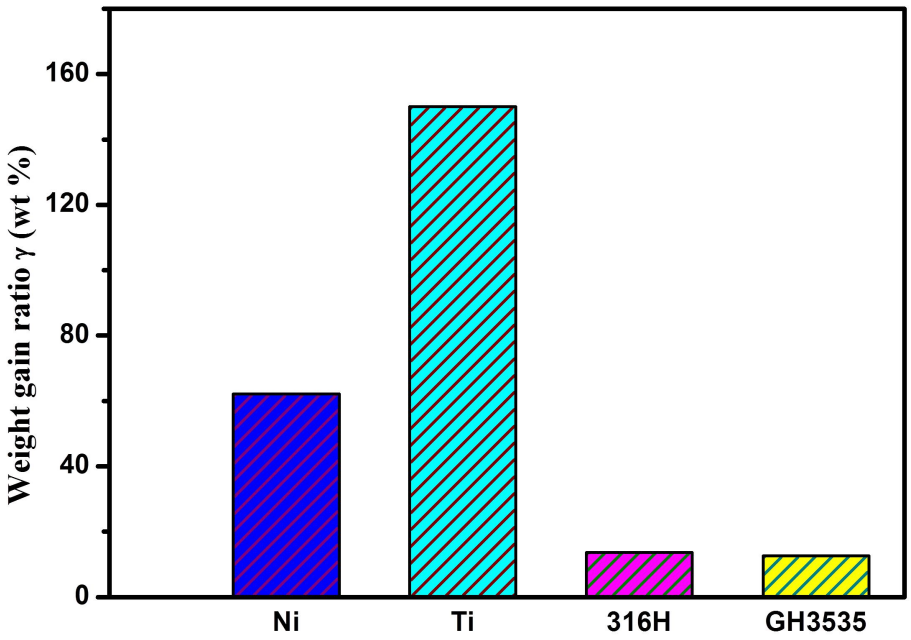

Fig. 2. Weight gain ratio of pure metals (Ni and Ti) and alloys (316H SS and GH3535) after corrosion in GaInSn at 650 °C for 5 h.

3.1 Corrosion behavior of Ni in GaInSn

Pure Ni metal exhibited significant corrosion, forming a thick reaction layer (Fig. 1(c)) even after a short immersion time of 5 h, indicating a potent interaction between Ni and GaInSn during immersion. The reaction layer exhibited a regular cruciform pattern on the initial square Ni substrate. A similar

corrosion morphology was also observed by Barbier et al. [32] when they immersed pure Ni into Ga at a lower temperature of 400 °C for 49 h.

The XRD patterns of the Ni sample immersed in liquid GaInSn at 650 °C for 5 h are shown in Fig. 3. The main peaks of Ni disappeared after corrosion, but the peaks of the Ni_2Ga_3 IMC with a small quantity of Ni_3Ga_4 were detected near the surface, indicating that the surface of the Ni matrix was entirely covered by Ni_2Ga_3 owing to the reaction of Ni with Ga at 650 °C. The formation of this reaction layer may explain the weight gain of Ni after corrosion. Moreover, no significant Ga, In, or Sn signals were detected via XRD, suggesting that GaInSn was completely removed from the sample during the cleaning process. According to the Ni–Ga binary phase diagram [36], binary Ni_2Ga_3 is the most stable phase at 650 °C. Hence, the reaction layer mainly consisted of stable Ni_2Ga_3 accompanied by a small quantity of metastable Ni_3Ga_4 owing to the short corrosion duration of 5 h in the immersion test.

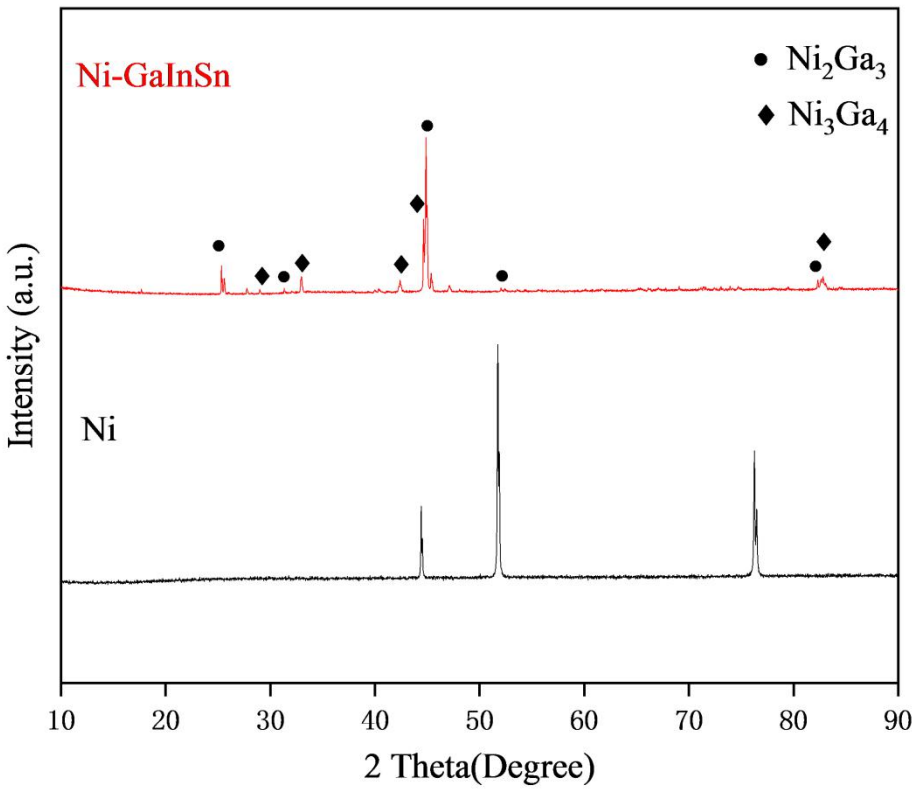

Fig. 3. XRD patterns of the Ni sample before and after corrosion in liquid GaInSn at 650 °C for 5 h.

The surface morphology and elemental distribution of the Ni sample after corrosion in liquid GaInSn at 650 °C for 5 h are illustrated in Figs. 4(a)–(i). The thickness of the reaction layer with a regular cruciform pattern that formed on the surface of the corroded Ni specimen was approximately 995–998 μm, corresponding to a dimension change ratio of 24.8%. These results demonstrated that Ni was significantly corroded by liquid GaInSn. Barbier et al. [32] reported that the morphology of the reaction layer directly depends on the properties of the elements diffused during growth, and that the thickness is influenced by the size of the specimen. Figs. 4(d) and (g) show the surface morphologies of the reaction

layer and matrix, respectively. The surface of the layer was densely distributed with large cylindrical particles. Conversely, the distribution of the cylindrical particles on the Ni matrix was sparse; however, many fine acicular particles were observed. The results of elemental mapping (Figs. 4(e)–(f) and (h)–(i)) and EDS points (Table 3) indicated that both the cylindrical particles on the reaction layer (marked as Point 1 in Fig. 4(b)) and the acicular particles on the Ni matrix (marked as Point 2 in Fig. 4(c)) after corrosion were rich in Ni and Ga, confirming that the reaction layer and substrate after corrosion mainly consisted of Ni_2Ga_3 IMC, which is consistent with the XRD analysis.

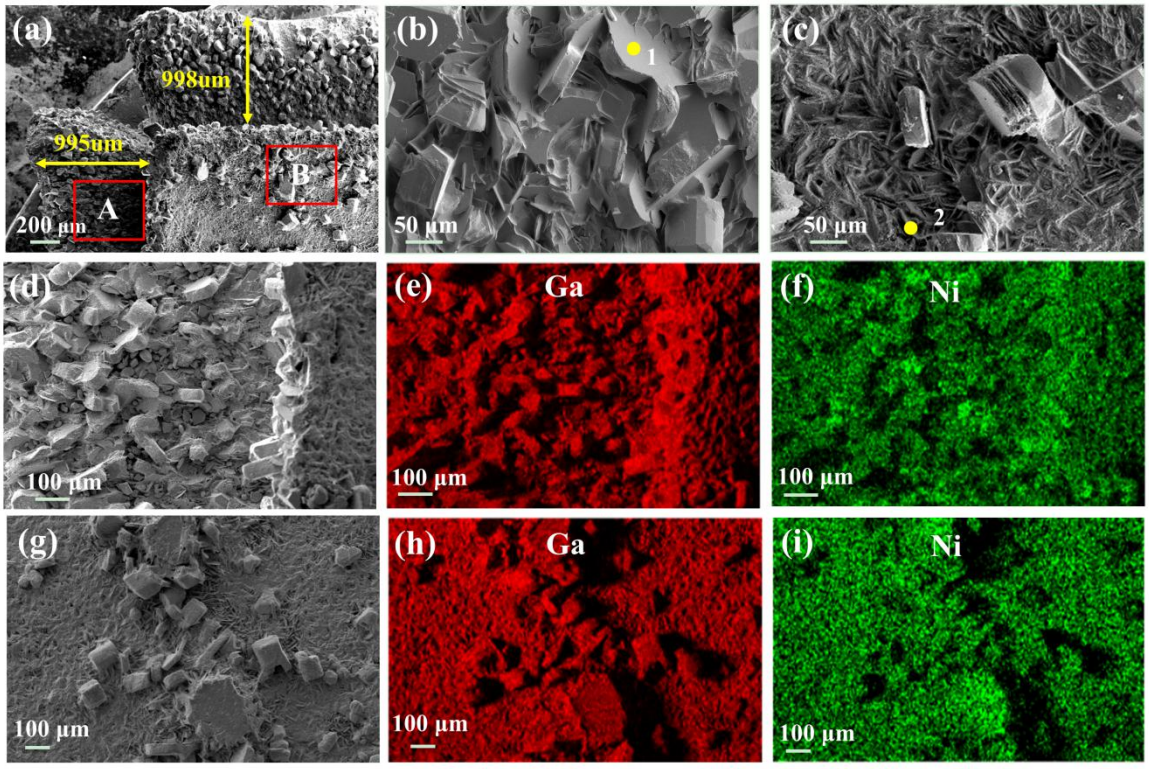

Fig. 4. (a) Surface morphology of the Ni sample corroded in liquid GaInSn at 650 °C for 5 h. (b) and (c) are the magnified SEM images of (d) and (g), respectively; (d) and (g) are surface morphologies of Areas A and B bounded by the red line in (a); (e) and (f) are the corresponding Ga and Ni EDS mappings of (d), respectively; and (h) and (i) are the corresponding Ga and Ni EDS mappings of (g), respectively.

Table 3 Chemical compositions of Points 1 and 2 in Figs. 4(b) and (c) (at.%).

	Ga	Ni	In	Sn
Point 1	60.8	39.2	-	-
Point 2	52.7	46.6	0.4	0.4

3.2 Corrosion behavior of Ti in GaInSn

As shown in Fig. 1(c), pure Ti metal exhibited the most severe corrosion after immersion in liquid GaInSn (as confirmed by its highest weight gain ratio among all the materials in Fig. 2). In contrast to pure Ni metal, no noticeable cruciform pattern was observed on the surface of Ti. Instead, bending deformation and even fracture occurred at the edges of the Ti specimen after LMC, indicating that severe corrosion in GaInSn leads to the embrittlement or failure of Ti.

The XRD patterns of the Ti sample before and after corrosion in liquid GaInSn at 650 °C for 5 h are shown in Fig. 5. For the corroded Ti sample, only a new binary $TiGa_3$ IMC was detected on the surface of the Ti matrix via XRD, indicating that the Ti surface was entirely covered by the corrosion product of $TiGa_3$.

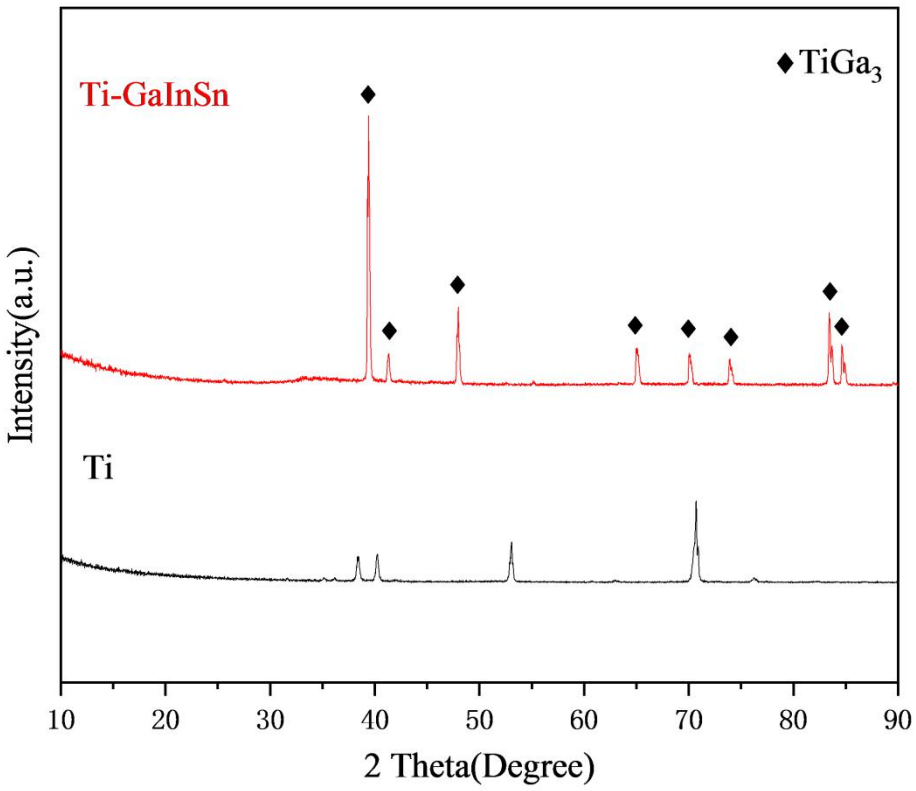

Fig. 5. XRD patterns of the Ti sample before and after corrosion in liquid GaInSn at 650 °C for 5 h.

The surface morphology and elemental distribution of the Ti sample after corrosion in liquid GaInSn at 650 °C for 5 h are shown in Figs. 6(a)–(d). The surface was curled with evident cracking, indicating that Ti was significantly corroded by liquid GaInSn. A surface tomography image of the crack region is shown in Fig. 6(b), and the corresponding elemental mapping is shown in Figs. 6(c) and (d). After corrosion, the surface of the Ti sample was covered with large polyhedral particles and large amounts of smaller particles, both of which consisted of Ga and Ti. In particular, many polyhedral particles were distributed at the edge of the cracking. SEM-EDS point analysis was conducted on a large

polyhedral particle and several smaller particles (marked as Points 1 and 2 in Fig. 6(b), respectively), the results of which are presented in Table 4. The polyhedral and smaller particles had almost the same Ga: Ti atomic ratio (3:1), which further confirmed that the $TiGa_3$ IMC was formed on the surface of Ti during corrosion.

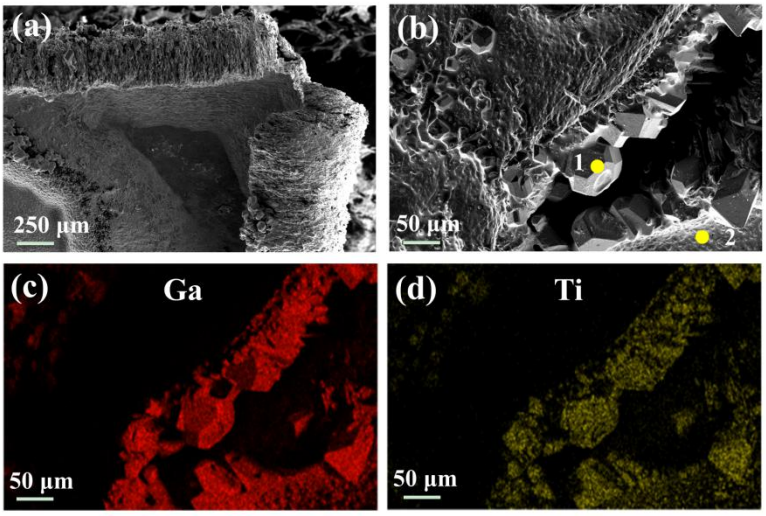

Fig. 6. (a) and (b) surface morphologies of the Ti sample corroded in liquid GaInSn at 650 °C for 5 h at different magnifications; (c) and (d) corresponding EDS mappings of (b).

Table 4 Chemical compositions of Points 1 and 2 in Fig. 6(b) (at.%).

	Ga	Ti	In	Sn
Point 1	76.2	23.7	-	-
Point 2	70.0	28.0	1.3	0.7

3.3 Corrosion behavior of 316H SS in GaInSn

316H SS exhibited better corrosion resistance than pure Ni and Ti metals, as shown in Figs. 1(c) and 2. Additionally, a relatively thinner reaction layer with a cruciform pattern was observed on the surface of 316H SS after corrosion.

The XRD patterns of the 316H SS sample before and after corrosion in liquid GaInSn at 650 °C for 5 h are shown in Fig. 7. After corrosion, the intrinsic peaks of 316H SS disappeared, and binary IMCs ($FeGa_3$ and $CrGa_4$) were detected, indicating the formation of new corrosion products. By analyzing the binary phase diagrams of the Fe–Ga [37] and Cr–Ga systems [38], the solubilities of Fe and Cr in liquid Ga were found to be very similar; therefore, either Fe or Cr in the 316H SS matrix react with Ga to form the corresponding binary IMCs $FeGa_3$ and $CrGa_4$, respectively.

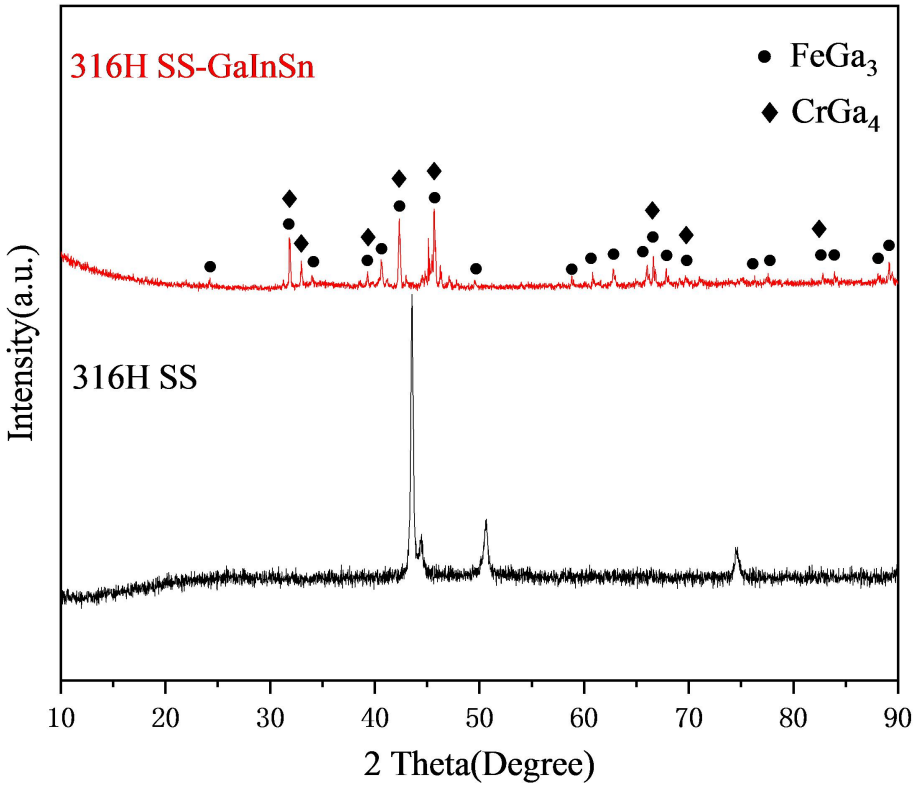

Fig. 7. XRD patterns of the 316H SS sample before and after corrosion in liquid GaInSn at 650 °C for 5 h.

The surface morphology and elemental distribution of 316H SS after corrosion in liquid GaInSn at 650 °C for 5 h are shown in Figs. 8(a)–(f). As shown in Fig. 8(a), a reaction layer was formed on the corroded 316H SS. Similar to Ni, the layer formed on 316H SS exhibited a regular cruciform pattern. Additionally, the layer formed from the short side (501.4 μm) of the original rectangular 316H SS substrate was similar to that formed from the long side (496.8 μm), leading to a dimensional change ratio of only approximately 9.8% for 316H SS, which was less than that of Ni (24.8%). The magnified surface morphologies and corresponding elemental distributions of the 316H SS matrix after corrosion

are shown in Figs. 8(d)–(f). Numerous corrosion products of varying sizes were distributed on the surface of the corroded 316H SS, which could be classified into three types. The first comprised fine particles (marked as Point 1 in Fig. 8(b)) that adhered to the substrate and contained Fe and Ga, according to the EDS results. Second, polyhedral particles with a regular shape stacked atop the fine particles could be further classified into two types. The first type (marked as Point 2 in Fig. 8(b)) was rich in Fe and Ga, whereas the second type (marked as Point 3 in Fig. 8(b)) was rich in Cr and Ga. Combined with the XRD results shown in Fig. 7, these two types of polyhedral particles were identified as $FeGa_3$ and $CrGa_4$ IMCs, respectively. As shown in Table 1, the Fe content of 316H SS was considerably higher than that of Cr. Hence, the Fe atoms in the matrix were prone to diffuse to the surface of the sample and react with Ga, resulting in more $FeGa_3$ formed on the surface than $CrGa_4$. Based on the above results, the wetting properties of metal bonds may result in the formation of a dense corrosion layer consisting of irregular $FeGa_3$ particles, which becomes strongly bound to the steel surface [39].

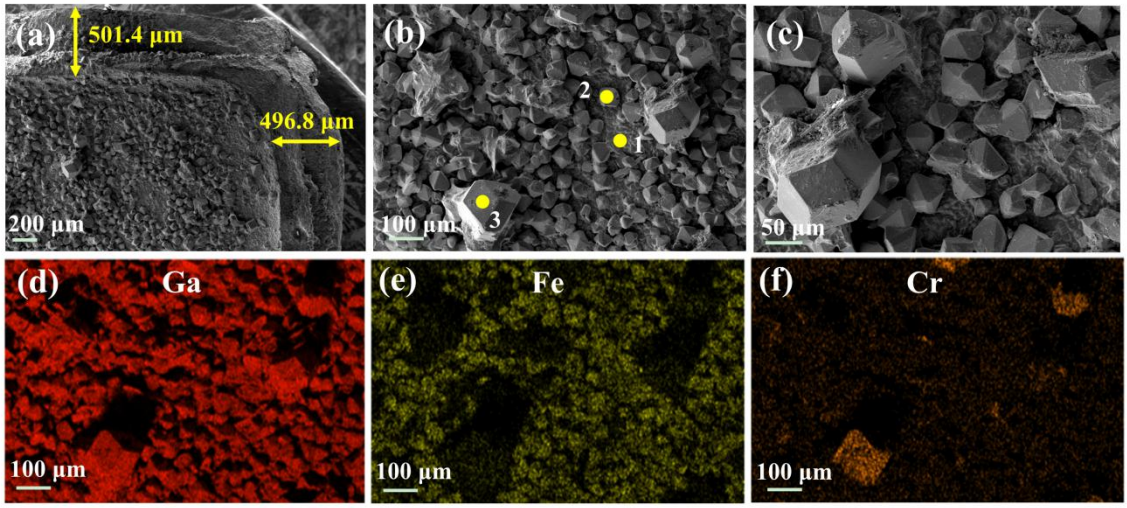

Fig. 8. (a) to (c) surface morphologies of the 316H SS sample corroded in liquid GaInSn at 650 °C for 5 h at various magnifications; (d)–(f) corresponding EDS mappings of (b).

Table 5 Chemical compositions of Points 1, 2, and 3 in Fig. 8(b) (at.%).

	Ga	Fe	Cr	In	Sn
Point 1	76.8	22.4	0.1	0.3	0.4
Point 2	75.7	24.0	0.1	0.1	0.1
Point 3	78.9	0.8	19.7	0.2	0.4

3.4 Corrosion behavior of GH3535 alloy in GaInSn

The GH3535 alloy exhibited better corrosion resistance than the other three materials, as evidenced by the absence of cruciform morphology, deformation, or cracks on the surface of the sample. Although several scattered corrosion particles were observed on the surface (Fig. 1(c)), they were negligible compared to the

other materials. Additionally, the lowest weight gain ratio observed in Fig. 2 further confirmed the excellent corrosion resistance of the GH3535 alloy. These results suggest that the GH3535 alloy is a highly viable and promising material for applications in harsh environments.

The XRD patterns shown in Fig. 9 reveal that the GH3535 alloy underwent corrosion in liquid GaInSn at 650 °C for 5 h. After corrosion, the characteristic diffraction peaks of the GH3535 alloy were entirely suppressed, and new features identified as $FeGa_3$ and Mo_6Ga_{31} IMCs were observed. The XRD results indicated that the surface of the GH3535 alloy sample was entirely covered by these two corrosion products after LMC.

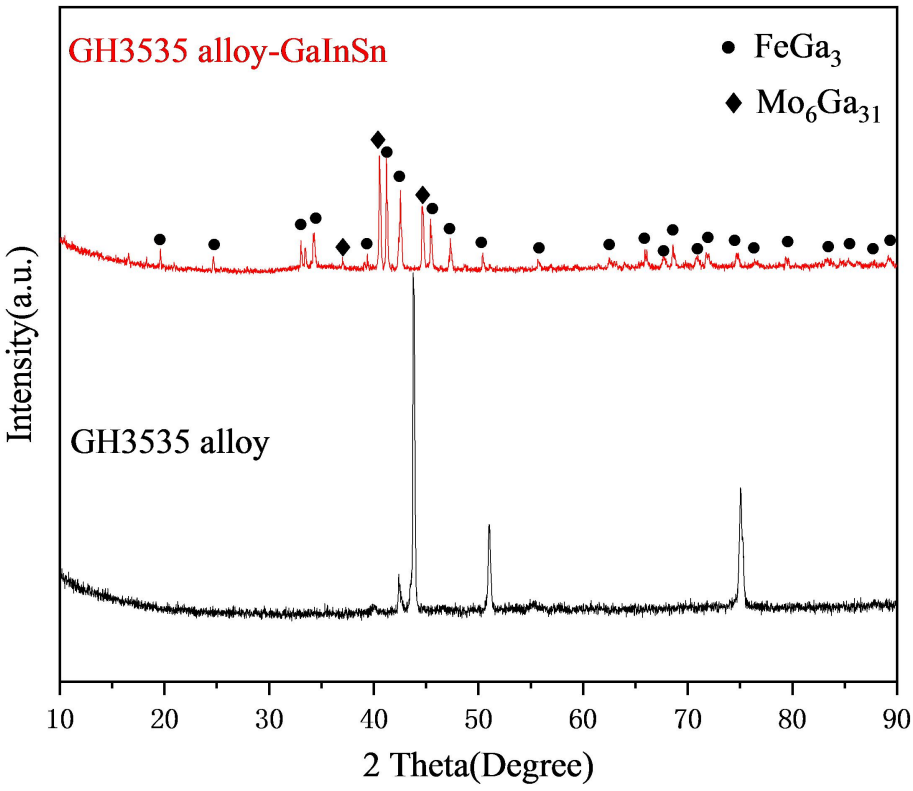

Fig. 9. XRD patterns of the GH3535 alloy sample before and after corrosion in liquid GaInSn at 650 °C for 5 h.

The surface morphologies and corresponding elemental distribution of GH3535 alloy after corrosion in liquid GaInSn at 650 °C for 5 h are shown in Figs. 10(a)–(f). The surface of the corroded GH3535 alloy was primarily covered with three types of IMCs. The bottom of the surface was densely packed with fine particles (marked as Point 1 in Fig. 10(b)), which were primarily composed of Mo and Ga, according to the EDS analyses. The top was dotted with several larger polyhedral particles (marked as Point 2 in Fig. 10(b)), which had a regular shape and were rich in Fe and Ga, as detected by EDS analyses. Strip-shaped particles (marked as Point 3 in Fig. 10(b)) were also observed on the surface adjacent to the fine particles, and the EDS results showed that they were rich in Ni and Ga. Based on the XRD results shown in Fig. 9, it could be inferred that the fine particles with a dense distribution at the bottom of the surface were the Mo_6Ga_{31} IMC, whereas the large polyhedral particles with a regular shape at the top were the $FeGa_3$ IMC. However, the strip-shaped particles rich in Ni and Ga could not be identified via XRD, possibly because of their low contents. EDS mapping showed that the surface of the corroded GH3535 alloy was rich in Mo, Fe, and Ga but poor in Ni, further indicating that the GH3535 substrate was covered with newly generated $FeGa_3$ and Mo_6Ga_{31} IMCs, which is consistent with the XRD results.

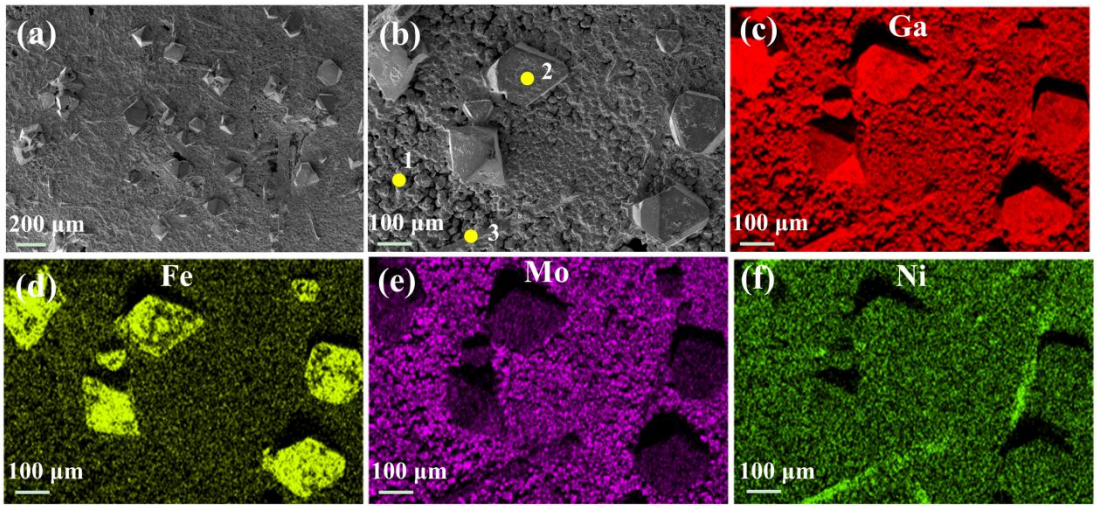

Fig. 10. (a) and (b) surface morphologies of the GH3535 alloy sample corroded in liquid GaInSn at 650 °C for 5 h; (c)–(f) corresponding EDS mappings of (b).

Table 6 Chemical compositions measured via SEM–EDS point analysis in Fig. 10(b) (at.%).

	Ga	Ni	Mo	Fe	Cr	In	Sn
Point 1	78.8	1.6	15.8	0.2	2.1	1.0	0.5
Point 2	73.7	0.4	0.1	24.4	0.1	0.9	0.4
Point 3	56.4	40.4	0.1	0.4	0.7	1.3	0.8

Figs. 11(a)–(g) show cross-sectional SEM images and the corresponding elemental distributions of the GH3535 alloy sample corroded in liquid GaInSn. The corrosion layer of the GH3535 alloy mainly consisted of two layers. The outer layer was severely depleted in Ni, Cr, and Fe, but rich in Mo and Ga,

indicating massive dissolution of metallic elements (Ni, Fe, and Cr) from the matrix to liquid GaInSn, as well as the inward diffusion of Ga into the matrix. The results obtained from the XRD patterns in Fig. 9 and the SEM images in Fig. 10 confirmed the existence of Mo–Ga and Fe—Ga IMCs on the surface of the GH3535 alloy after corrosion. However, no remarkable Ni–Ga IMC was detected in the XRD analysis of the corroded GH3535 alloy (Fig. 9). Only a few strip-shaped particles corresponding to the Ni_2Ga_3 IMC were embedded in the Mo-rich layer, as observed using SEM (Fig. 10). It is speculated that the Ni_2Ga_3 IMC has very weak adhesion to the GH3535 matrix and is likely to peel off because of the stress that occurs during the interaction between the solid and liquid phases or the difference in the thermal expansion coefficient between the Ni_2Ga_3 IMC and the alloy during the cooling process. The outer Mo-rich layer consisting of the Mo_6Ga_{31} IMC had a thickness of approximately 153 μm. The inner corrosion layer with a thickness of approximately 45 μm was visible between the outer Mo-rich layer and the matrix. The total thickness of the corrosion layer for GH3535 was approximately 197 μm. The Ni, Cr, Mo, and Fe contents were higher in the inner corrosion layer than in the outer Mo-rich layer but lower than those in the matrix. However, the Ga content was relatively lower in the inner corrosion layer than in the outer Mo-rich layer and decreased to zero in the matrix. This implies that the outer Mo-rich layer prevented the diffusion of Ga into the GH3535 matrix and metallic elements (Ni, Cr, and Fe) into the surface of the alloy. Therefore, the formation of this outer Mo-rich layer may alleviate the LMC of the GH3535 alloy

in GaInSn. This is reasonable because Mo exhibits lower solubility and reactivity than Ni, Fe, and Cr in liquid Ga, according to a previous report [40]. Miyakawa et al. [41] also reported the formation of Mo-rich and Cr-rich layers on the surface of the Hastelloy C276 matrix in liquid Sn, which beneficially influenced corrosion mitigation.

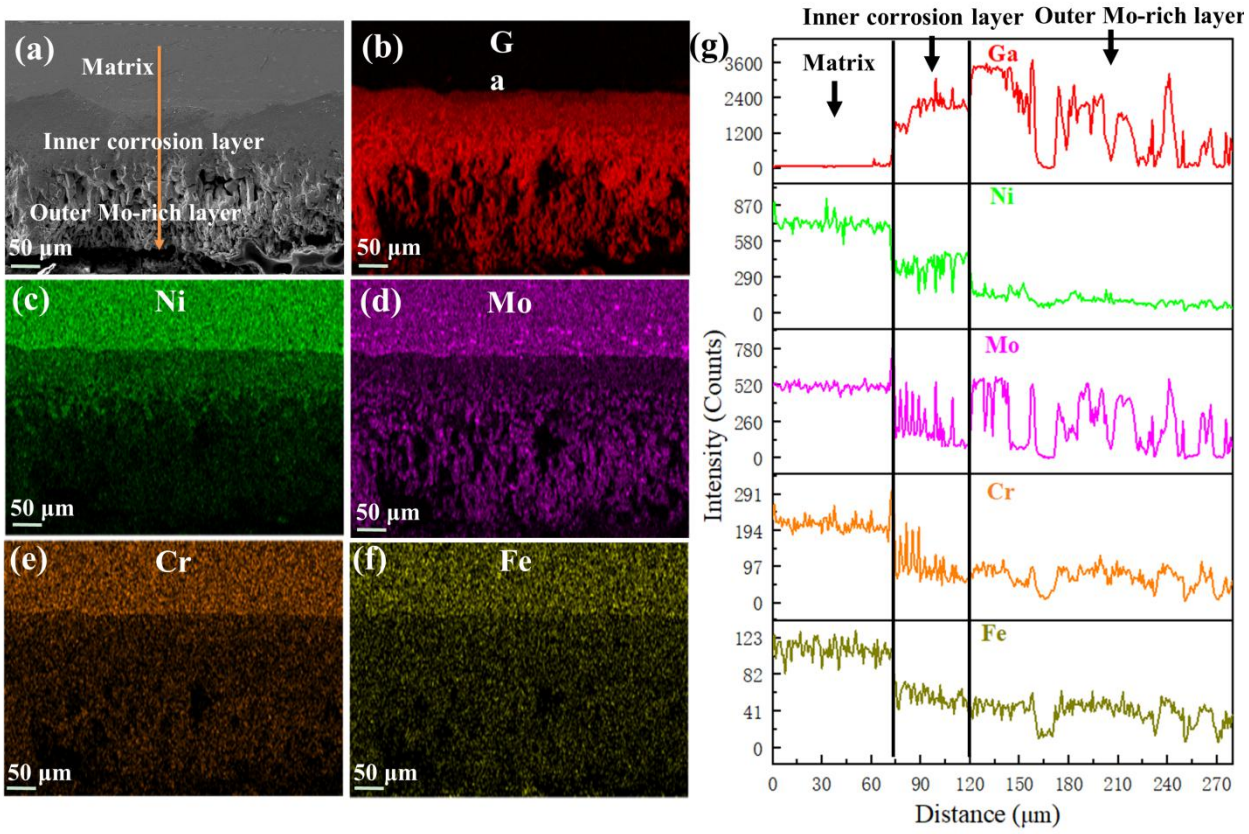

Fig. 11. (a) Cross-sectional morphologies of the GH3535 alloy sample corroded in liquid GaInSn at 650 °C for 5 h; (b)–(f) corresponding EDS mappings of (a); (g) corresponding EDS line-scan profile along the orange line in (a).

4 Discussions

After being exposed to liquid GaInSn at 650 °C for 5 h, all materials endured corrosion and exhibited weight gain because of the reactions between the metallic components in their bodies and Ga, leading to the formation of various binary Ga-rich IMCs on their surfaces. XRD analyses indicated that the surface of each sample was covered with newly generated IMCs.

It should be noted that only Ga-rich binary IMCs were detected on the surface of Ni, Ti, 316H SS, and GH3535 after corrosion in liquid GaInSn, and few compounds of In or Sn were detected via XRD. This was because Ga has a lower activation energy than Sn or In, which causes Ga atoms to preferentially diffuse toward and adhere to the surfaces of these materials. According to the results reported in literature, the diffusion activation energies of Ga, In, and Sn adsorbed on the W surface, as revealed by Nishikawa et al. [42], are 0.29 eV, 0.35 eV, and 0.71 eV, respectively. In addition, Saadat et al. [43] calculated the activation energies of Ga, In, and Sn on an Mo surface to be 0.25 eV, 0.3 eV, and 0.5 eV, respectively. Therefore, it can be inferred that Ga was selectively deposited onto the surface of these materials and reacted with metallic elements such as Fe, Ni, Cr, Ti, and Mo to form the corresponding binary $FeGa_3$, Ni_2Ga_3, $CrGa_4$, $TiGa_3$, and Mo_6Ga_{31} IMCs, respectively.

An important factor in determining the compatibility of a material with GaInSn is the solubility of its different elements in Ga. According to the literature [40, 44], the solubility of Ni, Fe, Cr, Ti, and Mo in liquid Ga at 400 °C is 0.59 at.%,

1.9×10^{-2} at.%, 1.2×10^{-2} at.%, 9.5×10^{-3} at.%, and 5.0×10^{-3} at.%, respectively. At 500 °C, the solubility increases for certain elements, with Ni, Fe, Cr, Ti, and Mo exhibiting a solubility of 1.35 at.%, 0.11 at.%, 4.9×10^{-2} at.%, 3.9×10^{-2} at.%, and 1.9×10^{-2} at.% in liquid Ga, respectively. It should be noted that the solubility of the elements in liquid Ga usually increases with temperature. Therefore, it can be inferred that at 650 °C, the elements in descending order of solubility in liquid Ga are Ni, Fe, Cr, Ti, and Mo. This is important for predicting the potential corrosion behavior of materials in GaInSn.

Based on the corrosion results shown above, pure metals (Ni and Ti) are more prone to corrosion in liquid GaInSn than the alloys (316H SS and GH3535). Specifically, Ti exhibited the largest weight gain ratio among all four materials, and its surface was observed to be completely distorted, as shown in Fig. 1(c), presumably because of the formation of the $TiGa_3$ IMC after LMC. In contrast, the reaction layer consisting of the Ni_2Ga_3 IMC along with a small quantity of Ni_3Ga_4 that formed on the surface of Ni exhibited a cruciform pattern along the substrate edges. The growth mechanism of the reaction layer formed on Ni is illustrated in Fig. 12. In the binary Ni–Ga system, the dominant diffusion of Ga into the Ni matrix led to the formation of the reaction layer on the surface of the Ni matrix. As the immersion time increased, the Ni substrate was partly peeled off by the reaction layer, beginning with the four edges of the initial square Ni substrate and gradually forming a cross-shaped pattern. These newly formed reaction layers led to severe

substrate deformation, with a corresponding dimensional change ratio of up to 24.8% after only 5 h of corrosion. The embrittlement and deformation of the metals observed after LMC imply that neither Ti nor Ni is suitable for use as a molten salt manometer diaphragm material. Corrosion-induced hardening or embrittlement would degrade the mechanical properties of a material.

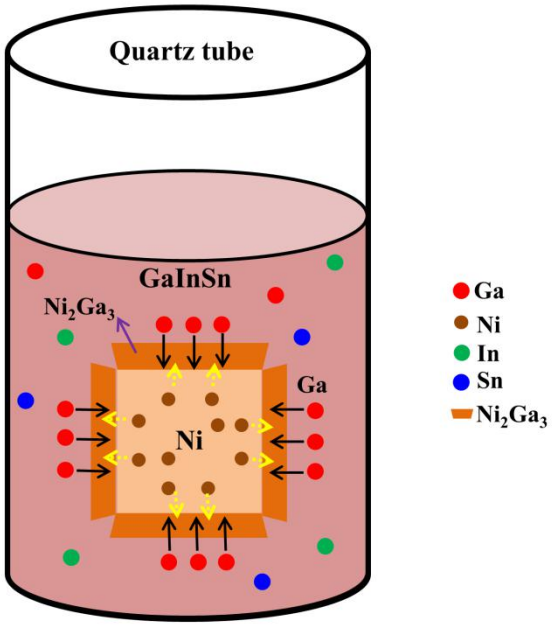

Fig. 12. Growth mechanism of the reaction layer formed on Ni.

Compared to pure metals (Ni and Ti), the alloys (316H SS and GH3535) exhibited relatively better corrosion resistance to liquid GaInSn. However, a high density of the $FeGa_3$ IMC and a small quantity of $CrGa_4$ were observed on the surface of 316H SS, which could potentially cause corrosion hardening and failure of the material in a liquid metal environment during long-term service. Furthermore,

a thin new reaction layer was formed on the four edges of 316H SS, the thickness of which was only half that of pure Ni, indicating a more severe reaction of Ni than that of Fe with liquid GaInSn. The reaction layer formed on 316H SS had a regular cruciform pattern similar to that of Ni, as shown in Fig. 8(a). Barbier et al. [32] reported the transition from a linear growth pattern with sharp corners to a parabolic pattern with rounded edges at the corners of the layer on 316 L SS with increasing immersion time, indicating that the kinetic regimes involved during the corrosion process changed from the initial interface-controlled mechanism to the later diffusion-controlled mechanism. During the 5-h corrosion experiment, the diffusion of Ga into the 316H SS matrix was dominant, leading to the formation of a reaction layer with a cross–shaped pattern on the surface of the 316H SS matrix. Guo et al. [45] found that the micro-hardness of the resulting $FeGa_3$ corrosion layer (7.63 ± 0.31 GPa) was significantly higher than that of the matrix (4.11 ± 0.41 GPa) during the reaction of T91 steel with a liquid GaInSn at 600 °C. Therefore, it is plausible to hypothesize that the formation of the $FeGa_3$ IMC on the surface of 316H SS after corrosion in GaInSn may contribute to an increase in the hardness of 316H SS. However, further studies are needed to confirm this hypothesis.

On the surface of GH3535 alloy, many Mo_6Ga_{31} and several $FeGa_3$ and Ni_2Ga_3 IMCs were observed. As shown in Table 1, although the constituent elements of the 316H SS and GH3535 alloys are similar, different types of binary Ga-rich IMCs were formed. This difference may be attributed to the content of the elements in the matrix and the solubility or reactivity of the elements in liquid Ga. The reaction of

Ni with liquid Ga was the most active among all constituent elements. However, very few Ni–Ga IMCs were found on the surface of the GH3535 alloy, which might be ascribed to the peeling of the Ni–Ga IMC formed on the surface during the cooling or cleaning process. Additionally, after immersion in liquid GaInSn, the surface $FeGa_3$ IMC, outer Mo-rich layer, inner corrosion layer, and matrix were clearly observed in the GH3535 alloy. Miyakawa [41] compared the corrosion behaviors of an iron-based alloy and nickel-based alloy in liquid Sn. Their results showed that elements with low reactivity easily formed enrichment layers on the alloy surface, which prevented elements with high reactivity in the matrix from diffusing to the surface to a certain extent, thus alleviating corrosion. Therefore, it is inferred that an enrichment layer of some elements was formed in both the Fe- and Ni-based alloys to alleviate corrosion. The corrosion resistances of the 316H SS and GH3535 alloys to the GLM were significantly better than those of pure metals (Ni and Ti).

However, a reaction layer was formed on the surface of 316H SS after corrosion, which is detrimental to the integrity and mechanical properties of the material during application. In comparison, the GH3535 alloy is more suitable as a candidate material for a pressure-sensing diaphragm because GH3535 alloy does not exhibit such a reaction layer. However, it should be noted that because the corrosion duration in this experiment was only 5 h, further investigation is necessary to evaluate the corrosion behavior of the GH3535 alloy in liquid GaInSn for longer corrosion durations.

5 Conclusion

In this study, the corrosion behavior of pure metals (Ni and Ti) and alloys (316H SS and GH3535) in liquid GaInSn was investigated via a static immersion test at 650 °C for 5 h. After corrosion, the mass change, phase structure, and morphologies of all the specimens were analyzed using weighing, XRD, and SEM-EDS characterization methods, and the following conclusions were obtained.

1. All specimens exhibited an increase in weight after immersion in GaInSn at 650 °C for 5 h, indicating that the decomposition of GaInSn and reactions between the metallic materials and GaInSn occurred during immersion. The corrosion resistance of the alloys (316H SS and GH3535) was significantly better than that of pure metals (Ni and Ti) in GaInSn.

2. After corrosion in GaInSn, various types of binary Ga-rich IMCs were formed on the metal and alloy surfaces. On the surface of Ni, the Ni_2Ga_3 IMC and a small quantity of Ni_3Ga_4 were formed, whereas the $TiGa_3$ IMC was formed on the surface of Ti. On the surface of 316H SS, the $FeGa_3$ IMC with a small quantity of $CrGa_4$ was detected, which is known to cause hardening of materials after long-term service. On the surface of the GH3535 alloy, a small quantity of $FeGa_3$ and a Mo-rich layer consisting of the Mo_6Ga_{31} IMC were found. Notably, reaction layers with a cruciform pattern were formed on the surfaces of Ni and 316H SS.

3. Given that the formation of reaction layers on the surface of 316H SS after corrosion is detrimental to its integrity and mechanical properties, the GH3535 alloy is a more favorable choice for a pressure conduction diaphragm. However, the

corrosion duration in this experiment was only 5 h, and further investigation is needed to investigate the corrosion behavior of the GH3535 alloy under extended durations.

Acknowledgments:

This study was supported by the National Natural Science Foundation of China (Grant Nos.12005289 and 52071331), the National Key R&D Program of China (Grant No. 2019YFA0210000), and the State Key Laboratory of Nuclear Detection and Electronics, University of Science and Technology of China (Grant No. SKLPDE-KF-202316).

Author contributions

All authors contributed to the study conception and design. Material preparation, data collection and analysis were performed by Jianhui Yu and Hongxia Xu. The first draft of the manuscript was written by Jianhui Yu. All authors commented on previous versions of the manuscript. All authors read and approved the final manuscript

References

[1] H.Z. Wang, S. Chen, B. Yuan et al., Liquid metal transformable machines. Acc. Mater. Res. **2**, 1227–1238 (2021). https://doi.org/10.1021/accountsmr.1c00182

[2] Q.Y. Wang, C.F. Pan, Y.X. Zhang et al., Magnetoactive liquid-solid phase transitional matter. Matter **6**, 855–872 (2023). https://doi.org/10.1016/j.matt.2022.12.003

[3] R. Matsuzaki, K. Tabayashi, Highly Stretchable, Global, and Distributed Local Strain Sensing Line Using GaInSn Electrodes for Wearable Electronics. Adv. Funct. Mater. **25**, 3806-3813 (2015). https://doi.org/10.1002/adfm.201501396

[4] Y. Sohn, K.M. Chu, Flexible hybrid conductor comprising eutectic Ga-In liquid metal and Ag

nanowires for the application of electronic skin. Mater. Lett. **265**, 127223 (2020). https://doi.org/10.1016/j.matlet.2019.127223

[5] M.K. Zhang, S.Y. Yao, W. Rao et al., Transformable soft liquid metal micro/nanomaterials. Mater. Sci. Eng. R Rep. **138**, 1–35 (2019). https://doi.org/10.1016/j.mser.2019.03.001

[6] Y.L. Lin, J. Genzer, M.D. Dickey, Attributes, fabrication, and applications of gallium-based liquid metal particles. Adv. Sci. **7**, 2000192 (2020). https://doi.org/10.1002/advs.202000192

[7] M.D. Dickey, Stretchable and Soft Electronics using Liquid Metals. Adv. Mater. **29**, 1606425 (2017). https://doi.org/10.1002/adma.201606425

[8] J. Touronen, M. Männistö, D. Richon et al., Application of GaInSn Liquid Metal Alloy Replacing Mercury in a Phase Equilibrium Cell: Vapor Pressures of Toluene, Hexylbenzene, and 2-Ethylnaphthalene. J. Chem. Eng. Data **65**, 3270–3276 (2020). https://doi.org/10.1021/acs.jced.9b01208

[9] D.H. Kim, J.A. Rogers, Stretchable Electronics: Materials Strategies and Devices. Adv. Mater. **20**, 4887-4892 (2008). https://doi.org/10.1002/adma.200801788

[10] N.B. Morley, J. Burris, L.C. Cadwallader et al., GaInSn usage in the research laboratory. Rev. Sci. Instrum. **79**, 056107 (2008). https://doi.org/10.1063/1.2930813

[11] G.L. Yun, S.Y. Tang, S.S. Sun et al., Liquid metal-filled magnetorheological elastomer with positive piezoconductivity. Nat. Commun. **10**, 1300 (2019). https://doi.org/10.1038/s41467-019-09325-4

[12] T. Daeneke, K. Khoshmanesh, N. Mahmood et al., Liquid metals: fundamentals and applications in chemistry. Chem. Soc. Rev. **47**, 4073-4111 (2018). https://doi.org/10.1039/C7CS00043J

[13] Q. Li, B.D. Du, J.Y. Gao et al., Liquid metal gallium-based printing of Cu-doped p-type Ga_2O_3 semiconductor and Ga_2O_3 homojunction diodes. Appl. Phys. Rev. **10**, 011402 (2023). https://doi.org/10.1063/5.0097346

[14] Q. Li, B.D. Du, J.Y. Gao et al., Room-Temperature Printing of Ultrathin Quasi 2D GaN Semiconductor via Liquid Metal Gallium Surface Confined Nitridation Reaction. Adv. Mater. Technol. **7**, 2200733 (2022). https://doi.org/10.1002/admt.202200733

[15] Q. Zhang, Y. Zheng, J. Liu, Direct writing of electronics based on alloy and metal (DREAM) ink: A newly emerging area and its impact on energy, environment and health sciences. Front. Energy **6**, 311-340 (2012). https://doi.org/10.1007/s11708-012-0214-x

[16] X.K. He, T.T. Xuan, J.P. Wu et al., Flexible and stretchable elastomer composites based on lightweight liquid metal foam spheres with pod-like contacts. ACS Appl. Mater. Interfaces **15**, 5856–5869 (2023). https://doi.org/10.1021/acsami.2c19621

[17] J.H. So, J. Thelen, A. Qusba et al., Reversibly Deformable and Mechanically Tunable Fluidic Antennas. Adv. Funct. Mater. **19**, 3632-3637 (2009). https://doi.org/10.1002/adfm.200900604

[18] A.A.Shirzadi, A.Laik, R.Tewari et al., Gallium-assisted diffusion bonding of stainless steel to titanium;microstructural evolution and bond strength. Materialia **4**, 115–126 (2018). https://doi.org/10.1016/j.mtla.2018.09.009

[19] F. Alnaimat, Y. Rashid, Thermal Energy Storage in Solar Power Plants: A Review of the Materials, Associated Limitations, and Proposed Solutions. Energies **12**, 4164 (2019). https://doi.org/10.3390/en12214164

[20] W.J. Ding, A. Bonk, T. Bauer, Corrosion behavior of metallic alloys in molten chloride salts for thermal energy storage in concentrated solar power plants: a review. Front. Chem. Sci. Eng. **12**, 564–576 (2018). https://doi.org/10.1007/s11705-018-1720-0

[21] A. Ravi Shankar, S. Mathiya, K. Thyagarajan et al., Corrosion and microstructure correlation in molten LiCl-KCl medium. Metall. Mater. Trans. A **41**, 1815–1825 (2010). https://doi.org/10.1007/s11661-010-0223-5

[22] H. Li, X.Y. Yang, X.Z. Yin et al., Effect of chloride impurity on corrosion kinetics of stainless steels in molten solar salt for CSP application: experiments and modeling. Oxid. Met. **95**, 311–332 (2021). https://doi.org/10.1007/s11085-021-10025-y

[23] E. Hamdy, J.N. Olovsjö, C. Geers, Perspectives on selected alloys in contact with eutectic melts for thermal storage: Nitrates, carbonates and chlorides. Sol. Energy **224**, 1210-1221 (2021). https://doi.org/10.1016/j.solener.2021.06.069

[24] W.J. Ren, G. Muralidharan, D.F. Wilson et al., Considerations of Alloy N for Fluoride Salt-Cooled High-Temperature Reactor Applications. Paper presented at ASME 2011 Pressure Vessels and Piping Conference (Baltimore, Maryland, USA, July 17-21, 2011)

[25] J. Serp, M. Allibert, O. Beneš et al., The molten salt reactor (MSR) in generation IV: Overview and perspectives. Prog. Nucl. Energy **77**, 308-319 (2014). https://doi.org/10.1016/j.pnucene.2014.02.014

[26] L.C. Olson, J.W. Ambrosek, K. Sridharan et al., Materials corrosion in molten LiF–NaF–KF salt. J. Fluor. Chem. **130**, 67-73 (2009). https://doi.org/10.1016/j.jfluchem.2008.05.008

[27] H.X. Xu, Q. Liu, B. Leng et al., Non-uniform corrosion of UNS N10003 alloy induced by trace SO_4^{2-} in molten FLiNaK salt. Corros. Sci. **192**, 109802 (2021). https://doi.org/10.1016/j.corsci.2021.109802

[28] L. Jiang, X.X. Ye, D.J. Wang et al., Synchrotron radiation-based materials characterization techniques shed light on molten salt reactor alloys. Nucl. Sci. Tech. **31**, 6 (2019).

https://doi.org/10.1007/s41365-019-0719-7

[29] K.Wang, L. Jiang, X.X. Ye et al., Absorption effect of pure nickel on the corrosion behaviors of the GH3535 alloy in tellurium vapor. Nucl. Sci. Tech. **32**,140 (2021). https://doi.org/10.1007/s41365-021-00976-x

[30] C.J. Du, X.G. Hu, P.Y. Guo et al., Effect of Gd on neutron absorption properties and electrochemical corrosion behavior of Zr-Gd alloy in boiling concentrated HNO_3. Nucl. Sci. Tech. **34**, 36 (2023). https://doi.org/10.1007/s41365-023-01193-4.

[31] J. Hui, B.L. Zhang, T. Liu et al., Effects of impurity elements on SiC grain boundary stability and corrosion. Nucl. Sci. Tech. **32**, 125 (2021). https://doi.org/10.1007/s41365-021-00963-2

[32] F. Barbier, J. Blanc, Corrosion of martensitic and austenitic steels in liquid gallium. J. Mater. Res. **14**, 737-744 (1999). https://doi.org/10.1557/JMR.1999.0099

[33] S.H. Shin, J.J. Kim, J.A. Jung et al., A study on corrosion behavior of austenitic stainless steel in liquid metals at high temperature. J. Nucl. Mater. **422**, 92-102 (2012). https://doi.org/10.1016/j.jnucmat.2011.12.007

[34] J. Guo, J. Cheng, H. Tan et al., Ga-based liquid metal: Lubrication and corrosion behaviors at a wide temperature range. Materialia **4**, 10-19 (2018). https://doi.org/10.1016/j.mtla.2018.09.007

[35] J. Mingear, D. Hartl, Liquid metal-induced corrosion of nickel-titanium alloys by gallium alloys for liquid metal-enabled shape memory applications. Corros. Sci. **167**, 108524 (2020). https://doi.org/10.1016/j.corsci.2020.108524

[36] R.W. Cahn, Binary Alloy Phase Diagrams–Second edition. Adv. Mater. **3**, 628-629 (1991). https://doi.org/10.1002/adma.19910031215

[37] E.M. Summers, T.A. Lograsso, M. Wun-Fogle, Magnetostriction of binary and ternary Fe–Ga alloys. J. Mater. Sci. **42**, 9582-9594 (2007). https://doi.org/10.1007/s10853-007-2096-6

[38] A. Belgacem-Bouzida, Y. Djaballah, M. Notin, Calorimetric measurement of the intermetallic compounds Cr_3Ga and $CrGa_4$ and thermodynamic assessment of the (Cr–Ga) system. J. Alloys Compd. **397**, 155-160 (2005). https://doi.org/10.1016/j.jallcom.2005.01.026

[39] Y. Cui, F. Liang, S. Xu et al., Interfacial wetting behaviors of liquid Ga alloys/$FeGa_3$ based on metallic bond interaction. Colloid Surf. A-Physicochem. Eng. Asp. **569**, 102-109 (2019). https://doi.org/10.1016/j.colsurfa.2019.01.079

[40] S.P. Yatsenko, N.A. Sabirzyanov, A.S. Yatsenko, Dissolution rates and solubility of some metals in liquid gallium and aluminum. J. Phys. Conf. Ser. **98**, 062032 (2008). https://doi.org/10.1088/1742-6596/98/6/062032

[41] Y. Miyakawa, M. Kondo, Corrosion behaviors of various steels and nickel-based alloys in liquid Sn media. Nucl. Mater. Energy **30**, 101154 (2022). https://doi.org/10.1016/j.nme.2022.101154

[42] O. Nishikawa, A.R. Saadat, Field emission and field ion microscope study of Ga, In and Sn on W: Structure, work function, diffusion and binding energy. Surf. Sci. **60**, 301-324 (1976). https://doi.org/10.1016/0039-6028(76)90319-8

[43] A.R. Saadat, Activation energies for surface diffusion and polarizabilities of gallium, indium and tin on a molybdenum surface. J. Phys. D: Appl. Phys. **27**, 356 (1994). https://doi.org/10.1088/0022-3727/27/2/026

[44] S.P. Yatsenko, Y.A. Anikin, Solubility of metals of the fifth period in liquid gallium. Mater. Sci. **6**, 333-337 (1973). https://doi.org/10.1007/BF00720616

[45] J. Guo, J. Cheng, S. Wang et al., A Protective $FeGa_3$ film on the steel surface prepared by in-situ hot-reaction with liquid metal. Mater. Lett. **228**, 17-20 (2018). https://doi.org/10.1016/j.matlet.2018.05.111